Circling optical vortices

M. Vaupel and C. O. Weiss
Physikalisch-Technische Bundesanstalt, 38116 Braunschweig, Germany
(Received 14 November 1994)

Using a photorefractive oscillator, we show experimental optical patterns whose principal features are optical vortices moving around an optical axis on circles. These patterns can be interpreted as simultaneous emission of helical fields with high-charge phase singularities and other rotationally symmetric fields. Patterns with up to nine circling vortices are shown, as well as patterns with two concentric "wheels" of vortices. Mode locking in these rotating patterns corresponds to a stopping of the rotation. An intermediate case between free rotation and locking, in which the pattern "jumps" between certain angular positions, is demonstrated, showing that phase locking of these modes, which is not possible for an isotropic resonator, can come about by small anisotropies.

PACS number(s): 42.55.−f, 42.60.Fc, 42.50.Ne

I. INTRODUCTION

We have recently found that lasers can emit fields with moving vortices [1]. This was experimental evidence that vortices in lasers have particlelike properties, i.e., that they are entities which can move without disintegrating. In [1] the motion of a single vortex was followed indirectly by using two strategically placed point detectors. It would seem difficult to follow more complex dynamical patterns with this technique. As the typical time scale of this motion of lasers is 10^{-8} s, there exists no real possibility to record films or even snapshots of the time-varying laser field.

Photorefractive oscillators (PRO's) are, on the other hand, largely equivalent to lasers of class A [2]. Since their gain-line widths are of the order of hertz, they show an extreme frequency pulling which results in dynamics with a characteristic time of 100 ms. Thus dynamics can be observed with ordinary video equipment. The PRO permits one, then, to observe highly complex spatial dynamics of lasers, otherwise not accessible to observation. We have therefore carried out experiments on a PRO which generalize the observations of [1] to a larger number of circling vortices. As we work at low gain the differences between PRO's and lasers should be negligible [2] and the experiments should give a proper picture of spatial laser dynamics of an ordered type.

II. EXPERIMENTAL SETUP

Figure 1 shows the experimental setup. We use a ring resonator (perimeter 2 m) with an even number of mirrors. In a resonator with an odd number of mirrors, only symmetric modes can be excited.

The resonator consists of two plane dielectric mirrors $M4$ and $M3$ whose reflectivities are 90% and 98.5%, polarizing beam splitters (PBS), a $Bi_{12}SiO_{20}$ BSO crystal (length 10 mm, width 5×5 mm^2) as the active medium,

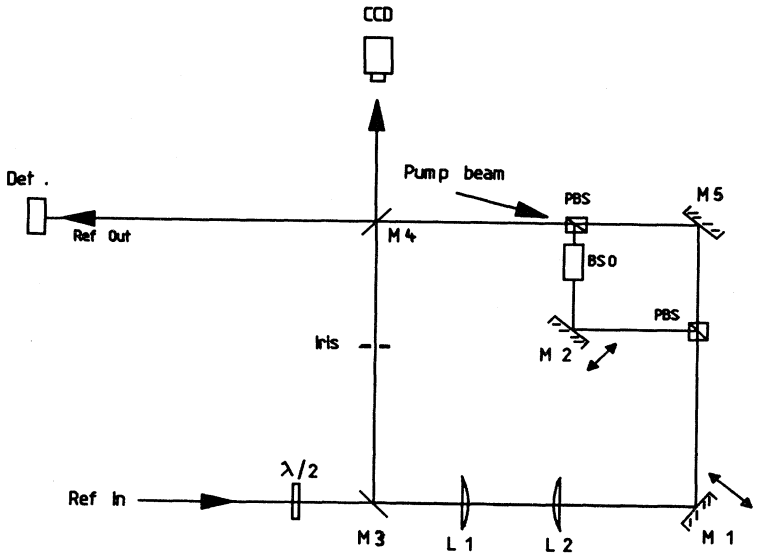

FIG. 1. Experimental setup. The active resonator is formed by four mirrors $M1$–$M4$ and the (active) BSO crystal. PBS is the polarizing beam splitter. The resonator formed by $M1$, $M3$, $M4$, and $M5$ has high finesse and is thus suitable for resonator length stabilization. The reference signal is provided by part of the pump radiation with polarization perpendicular to pump and generated fields.

plane mirrors ($M1$ and $M2$), both movable by a piezo, two lenses ($L1$ and $L2$), and an iris. The generated field is perpendicularly polarized relative to the resonator plane.

To excite reproducibly certain transverse-mode families, the resonator length is actively stabilized. A reference beam (Ref. In) with horizontal polarization counterpropagates to the generated field. A part of the pump radiation from an Ar^+ laser (514 nm) is used as the reference. Hence due to the PBS's the reference beam takes the path (length ≈ 8 cm) between the PBS's, which does not include the crystal. The reference field thus experiences a high-finesse resonator whose resonances are well suited to stabilize the resonator length. The path containing the BSO crystal is part of a very-low-finesse resonator which is unsuitable for stabilization; thus the division into an "active" and a "stabilization" resonator. The resonator is not absolutely stabilized in length but rather with reference to the pump radiation. The reason is the following. What is to be controlled is the tuning of the "active" resonator with respect to the PRO gain line. The latter is about 1 Hz offset from the pump frequency. Then the pump frequency is the proper reference for the measurements. If the pump frequency changes, the resonator changes with it.

The "active" resonator is stabilized actively using the reference signal (Ref. Out). To this end an ac voltage (1 kHz) on the piezo of mirror $M1$ modulates the total resonator length. The changes in transmission of the TEM_{00} resonance due to the modulation are phase-sensitively detected to stabilize the resonator length by the usual feedback technique.

The short path length between the PBS's including the crystal is not stabilized. However, the small ratio of this path length to the total round-trip length and the symmetric setup of both paths as well as mounting on an Invar plate and shielding from air currents limit the fluctuations between the two paths to the order of the acceptable MHz/min.

For optical amplification in the resonator, the BSO crystal is pumped through one of the PBS's by an Ar^+ laser whose intensity is around 0.3 mW/cm^2. The pump beam propagates at an angle of $\simeq 0.8°$ to the direction of the generated field for optimum amplification. The whole crystal is uniformly (within 5%) illuminated. To achieve this, the BSO is located at a distance of only 1 cm from the PBS. The last requirement for gain is a dc voltage V_0 on the crystal (5–5.5 kV), because BSO is a drift-type photorefractive material [3].

Transverse patterns depend on the properties of the resonator. These properties depend in our case on the focal lengths of the two lenses ($L1$ and $L2$) and the distance between them. By a selection of the focal lengths and the distance we set the resonator parameters g_1 and g_2, that is, the location in the stability diagram and the transverse-mode spacing. This determines the number of transverse modes per free spectral range (FSR) (150 MHz). It is possible to determine the frequencies of the transverse modes of the resonator without the crystal: One can record the transmitted reference intensity as a function of the piezo voltage, the latter being approximately proportional to the frequency of the resonator. Figure 2 gives an example for the case of approximately four transverse-mode spacings per FSR. Higher-order modes are discriminated by diffraction, meaning that they have less transmission and larger linewidth. The iris is used to control the losses of the modes so that we select the highest excitable transverse mode by its aperture. The finesse of the passive resonator without the crystal is larger than 40 with open iris. In the active resonator containing the crystal the high loss of the crystal ($\alpha = 1-2$ cm^{-1}) decreases the finesse to 2.8–5.4.

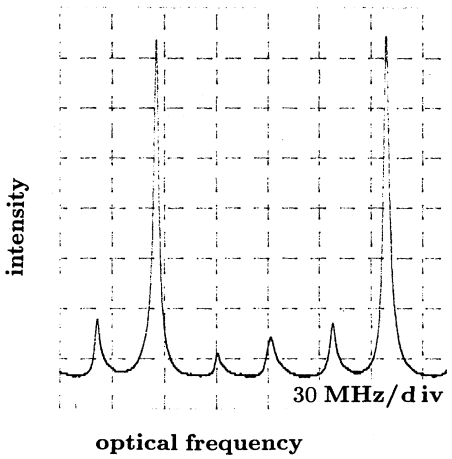

FIG. 2. Transmission of the resonator without BSO crystal, showing the transverse-mode resonances.

We achieve transverse-mode selection by moving the mirror $M2$ with a piezo. This change in resonator length is not compensated by the active stabilization but moves the mode frequencies relatively to the gain line of the crystal. Hence the dc voltage of the piezo on $M2$ determines which modes are excited.

10% of the generated field is coupled out and recorded by a charge-coupled device (CCD) camera.

III. DOUGHNUT MODES

In this section we describe "doughnutlike" patterns which are essentially bright fields with a dark center at the optical axis. The optical field of those patterns contains a phase singularity (also called a vortex). We observed doughnutlike patterns with phase singularities of order up to 15.

Often the vortices of these patterns do not exist exactly on the optical axis but close to one another near this axis. The "doughnut" order which equals the number of vortices is their transverse-mode family order.

Pure doughnutlike patterns of order n typically appear if the resonator has at least $n+1$ excitable transverse-mode families per FSR. Then an order-n doughnut is usually obtained by exciting the corresponding transverse-mode family without simultaneous excitation of the other transverse-mode families.

For the measurements we used a near-concentric resonator with ten transverse modes pre FSR. Using the piezo on $M2$ we select the transverse-mode family whose

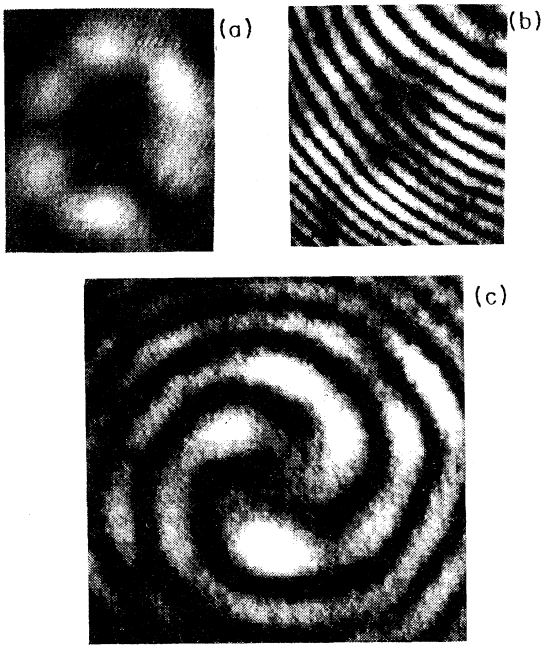

FIG. 3. Pattern with three phase singularities (vortices): (a) intensity, (b) interferogram with dislocations at the vortex locations, and (c) "spiral" interferogram of pattern with charge-3 phase singularity.

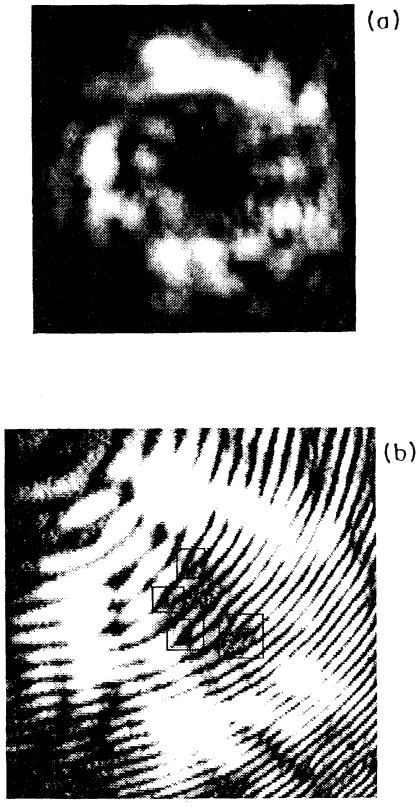

FIG. 4. Pattern with five phase singularities (vortices): (a) intensity and (b) interferogram with dislocations at the vortex locations.

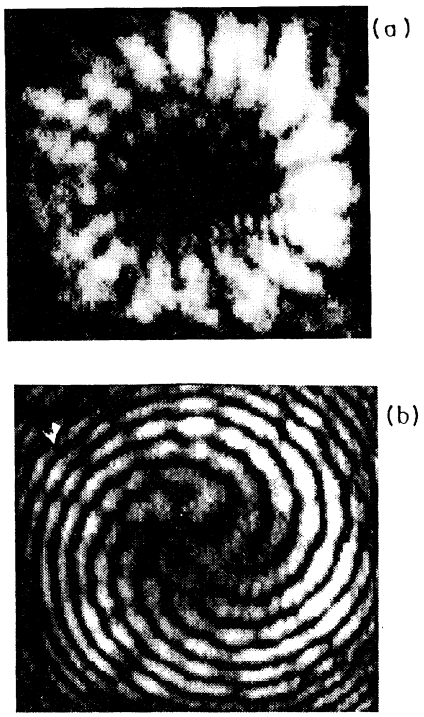

FIG. 5. Pattern with nine phase singularities (vortices): (a) intensity and (b) "spiral" interferogram of pattern with charge-9 phase singularity.

doughnut pattern is to be excited. Figures 3(a), 4(a), and 5(a) show the observed static patterns for mode families 3, 5, and 9 as examples. These pattern are essentially bright ringlike structures with a dark center, although residues of "flower" Laguerre patterns are still apparent.

If we superpose the patterns with a near-plane wave [4], e.g., with a part of the pump-laser radiation, we observe dislocations in the interference fringe pattern due to the phase singularities. These dislocations appear in the dark center of the intensity pattern. Corresponding to Fig. 3(a), Fig. 3(b) shows a charge-2 vortex in the center where three interference lines merge into one. A charge-1 singularity is located below. The total topological charge of the dark center equals the transverse-mode order of 3. Figure 4(b) shows the interference picture of a charge-5 doughnut corresponding to Fig. 4(a).

Another interference representation is suitable to stress the symmetry: interference between the pattern and a spherical wave realized by a laser beam after passing through a concave lens. Figures 3(c) and 5(b) show this in the case of charge-3 and -9 singularities. The charge corresponds to the number of spiral arms.

Other patterns different from these doughnuts can be emitted by introducing astigmatism or by using a larger iris. Using a small iris aperture, doughnuts are emitted predominantly.

IV. CIRCLING VORTICES

A. Beat between a doughnut and a Gaussian mode

Simultaneous excitation of a doughnut and a Gaussian mode results in a circular motion of the vortex as was

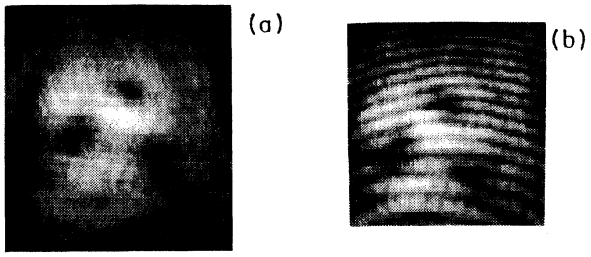

FIG. 6. Snapshot of three circling vortices: (a) intensity and (b) interferogram.

previously demonstrated on a Na_2 laser [1]. Corresponding to the circling of one vortex in [1] would expect circling of n vortices for a charge-n doughnut field.

We obtain three circling vortices in a resonator with nearly three transverse mode spacings per FSR if we excite the third mode simultaneously with the Gaussian mode. Figure 6 shows the result. The Gaussian pushes the vortices away from the center and they circle with a frequency that is the difference between the pulled frequencies of the active modes. Alternatively to a mode picture, one can also understand this behavior in a hydrodynamic picture [5]. From this the motion of the vortex is caused by two forces. One is proportional to the intensity gradient (as buoyancy) and pushes the vortex radially away from the center. The second force (Magnus force) causes the circling. It is due to "rotation" of the vortex. Lacking better ways of showing motion in a journal, we show in Fig. 7 the intensity in two locations of the transverse plane which lie on the orbit of the vortices. The phase shift between the two curves demonstrates the circling.

We obtained five circling vortices using nearly five transverse-modes spacings per FSR (Figs. 8 and 9); and nine circling vortices using a resonator with nearly nine transverse modes (Figs. 10 and 11). These examples show that this circling is a general form of dynamics. We have observed patterns with up to 15 circling vortices.

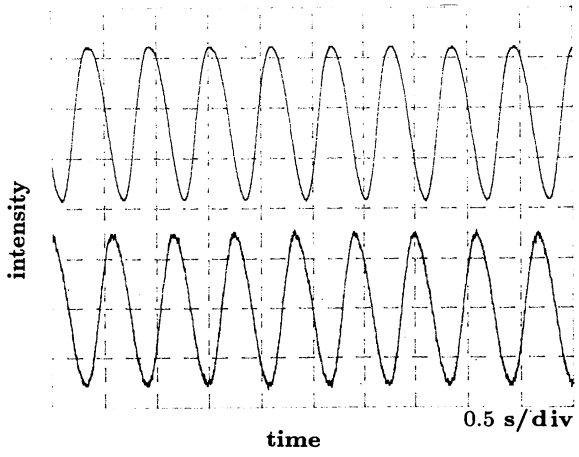

FIG. 7. Intensity at two different points of vortex trajectory (phase delay shows the motion of the vortices).

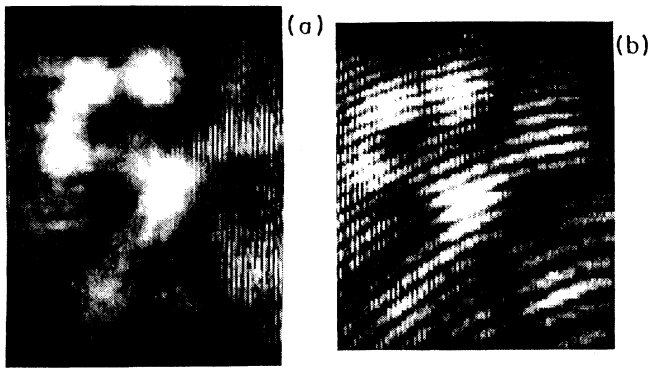

FIG. 8. Five circling vortices (snapshot): (a) intensity and (b) interferogram.

B. Hysteresis between circling directions

We investigated the case of approximately 4.1 transverse-mode spacings per FSR. When the gain line lay between the zeroth- and the fourth-order mode four vortices circled (Fig. 12). Tuning the Gaussian mode close to the gain line was found to decrease the speed of circling or to stop the circling motion. Figure 13 shows the revolution times for different detunings. Figure 13(a) shows measurements while tuning the Gaussian away and the fourth-order mode towards the gain line. Figure 13(b) give the measurements when tuning in the opposite direction. The uncertainties in detuning arise from the fluctuations of the short nonstabilized path of the resonator.

The transverse and the fundamental mode have different frequency pulling. The pulling depends on the losses of a mode. The fourth-order mode has higher losses than the TEM_{00} due to the iris. Thus the circling speed can be controlled by the resonator tuning. As one might expect the revolution time shows a dispersion-type dependence on the tuning. When the two modes phase lock, four stationary vortices result.

As we tune the Gaussian away and the fourth-order-mode family towards the gain line we find that the right-

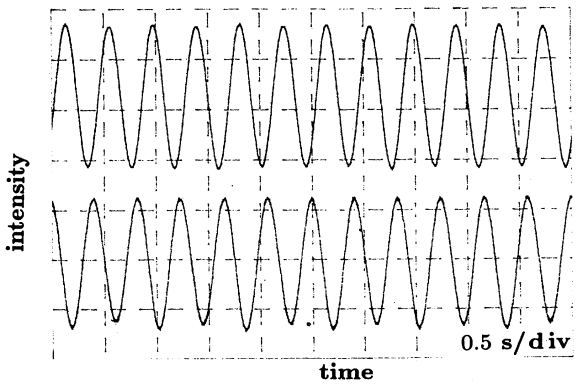

FIG. 9. Intensity at two different points of vortex trajectory corresponding to Fig. 8. Phase delay shows circling motion of the vortices.

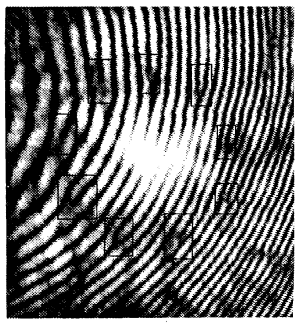

FIG. 10. Nine vortices circling (snapshot): (a) intensity and (b) interferogram.

hand circling changes to left-hand circling at a particular detuning corresponding to a circling frequency of $\simeq 0.45$ Hz. Figure 14 shows this by giving again the intensity in two points on the circle of vortex motion as the transition point is crossed. During the transition the phase difference between the two traces changes from $\pi/2$ into $-\pi/2$, meaning reversing of the circling direction. In addition, the amplitude and the mean intensity have changed. This may be caused by a change of the radius of

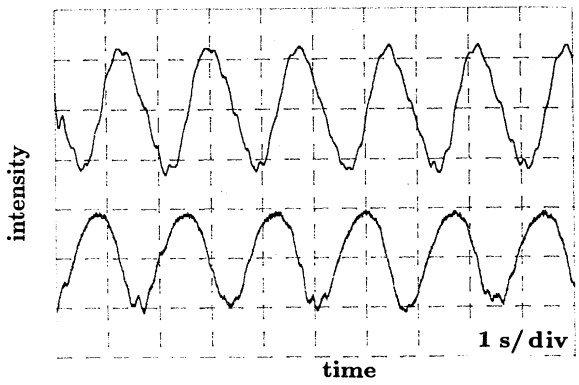

FIG. 11. Intensity at two different points on the vortex trajectory of nine vortices showing the circling motion.

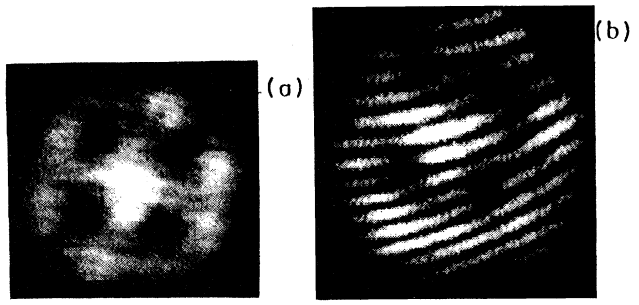

FIG. 12. Four circling vortices (snapshot): (a) intensity and (b) interferogram.

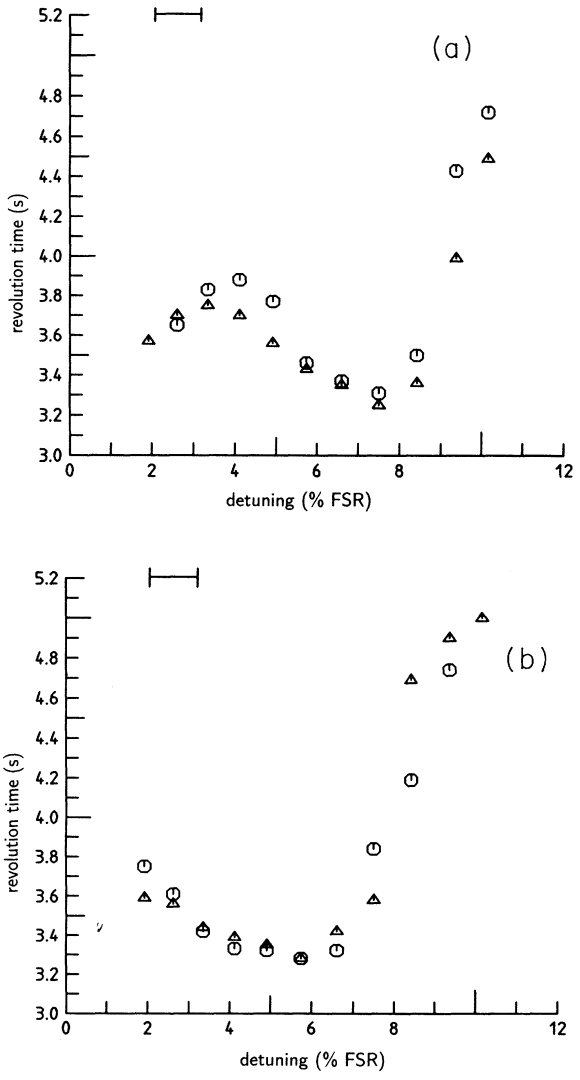

FIG. 13. Revolution time as a function of detuning, for four vortices. The dependence on the detuning results from the different frequency pulling of the constituent modes. (a) Measured while tuning from zeroth mode towards fourth mode and (b) measured while tuning back towards zeroth mode.

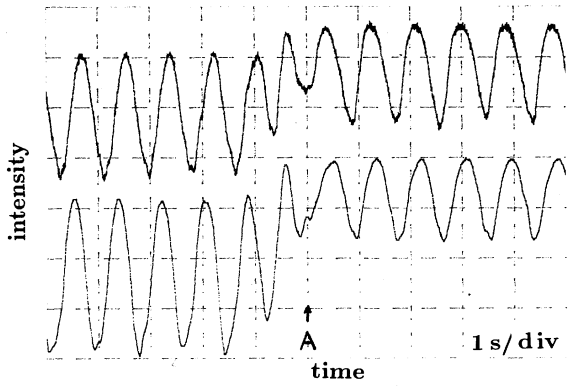

FIG. 14. Intensity in two points of the four-vortex rotating pattern showing reversal of circling direction at point A.

the vortex trajectory circle.

Tuning the Gaussian back towards the gain line, a second transition point is found at a circling frequency of $\simeq 0.096$ Hz, where a change back into right-hand circling occurs. A detuning difference of 10% of FSR between these two points was measured, indicating hysteresis. We can rule out that this hysteresis is simply caused by a possible mechanical hysteresis of the piezo, by using the circling frequency as a measure for the detuning rather than the piezo voltage.

The fourth-order doughnut can have vortices of positive or negative helicity. The sign of the helicity determines the direction of circling. We find correspondingly that at the points where the circling direction changes the helicity of the four vortices changes. It is plausible that there should be a hysteresis between circling directions because patterns are bistable with respect to helicity [6]. What causes the pattern at particular detunings to change the sign of their topological charge is unclear to us at present. We note, however, that outside the hysteresis region the helicity is uniquely determined by the tuning, i.e., the laser has a preference for a particular helicity, which is surprising since some sort of "helical astigmatism" of a resonator would seem an unusual property.

C. Mode locking

While here there is hysteresis between circling directions, it is also possible to phase-lock the two modes. This corresponds to stopping of the circling motion and occurs when the modes are tuned so that their pulled frequencies become close enough. Close to the locking point one observes that the circling motion becomes nonuniform. The four vortices remain at certain angular positions longer than between them. Figure 15 shows this by the intensity, measured again at one point of the circular vortex trajectory. The dwell time at these angular positions increases as the locking point is approached. When crossing the locking point the sense of circling obviously changes, while the sign of the helicity of the vortices is maintained.

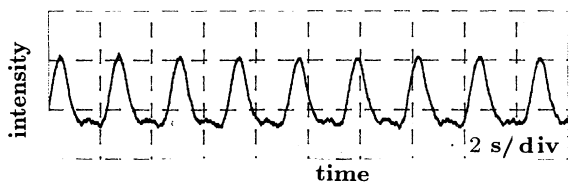

FIG. 15. The four-vortex pattern close to phase locking. Intensity at one point of the vortex trajectory. The vortices dwell a long time at a particular angular position.

In principle, this kind of phase locking is unexpected. The phase difference between the modes determines the orientation of the pattern. Since all orientations are equally probable there should be no restoring force for a particular phase and hence no mode locking. The only imaginable reason for the stopping of the circling (and thus the mode locking) is a resonator anisotropy, which favors certain orientations of the pattern. Consequently, we found that radial introduction of a pin permitted us easily to stop the circling motion.

D. Simultaneous excitation of higher-order doughnut modes with a first-order doughnut mode

Here we show that interference with a Gaussian mode is not necessary for vortices circling. Using a resonator of 2.7 ± 0.1 transverse-mode spacings per FSR, patterns like a stationary first-order vortex at the center with seven circling vortices around (Fig. 16) arise. One can

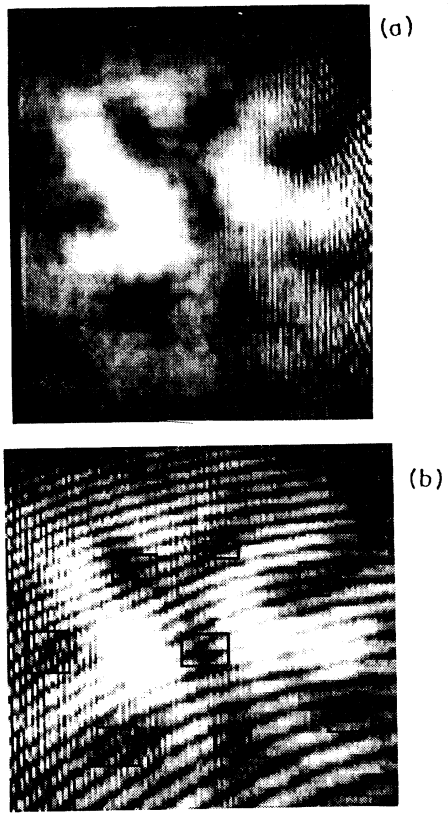

FIG. 16. Seven vortices circle around a central vortex (snapshot). The central vortex has topological charge opposite to the circling vortices. (a) intensity and (b) interferogram.

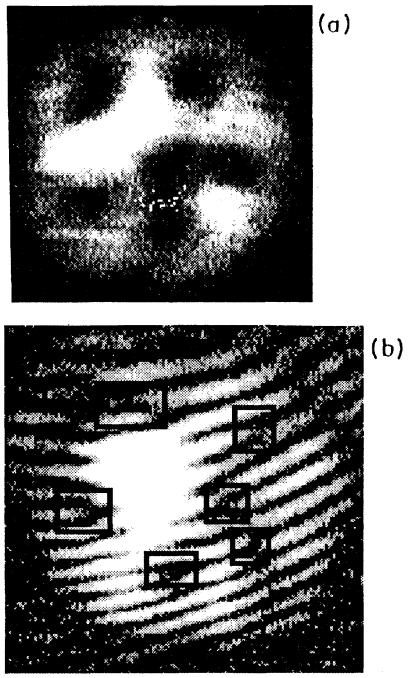

FIG. 17. Five vortices moving on an outer circle and one vortex moving in the same sense on a smaller circle concentric with the outer circle (snapshots). Topological charge of inner moving vortex opposite to outer vortices: (a) intensity and (b) interferogram.

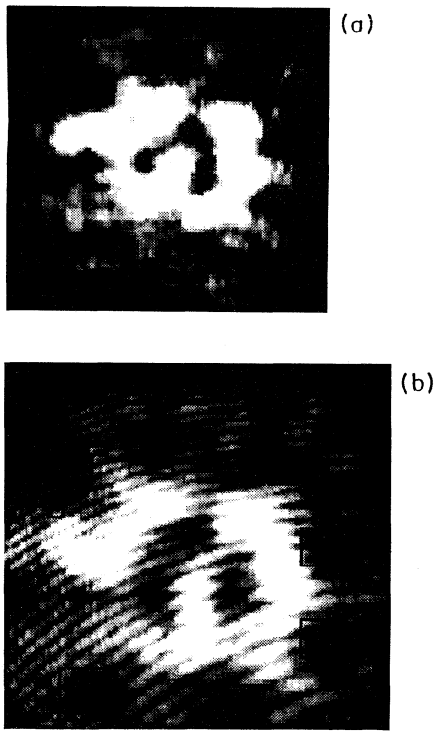

FIG. 19. Three vortices moving on an inner circle and eight vortices moving on an outer circle (snapshots): (a) intensity and (b) interferogram.

construct this pattern by interference between a charge-1 and a charge-6 doughnut. Note that this leads to seven circling vortices and one stationary central vortex.

V. THREE-MODE EXCITATION

In a similar way one can obtain one vortex moving on a circle with five vortices moving on a concentric outer circle by simultaneous excitation of TEM_{00}, first-order, and fourth-order doughnuts (Fig. 17). Figure 18 gives the corresponding intensity of one detector placed on the inner circle (upper trace) and another one on the outer circle (lower trace). The amplitude variations of the peaks of the lower curve arise because the inner vortex also touches this detector slightly.

As a last example we show the case of simultaneous excitation of a charge-3 and a charge-5 doughnut together with the fundamental mode (Fig. 19). Three vortices move on a circle of a small radius while eight vortices move at a large distance from the optical axis. Figure 20 shows again the intensity as a function of time on the inner circle (upper trace) and on the outer circle (lower trace). The ratio of the two circling frequencies is nearly $\frac{9}{16}$. This ratio corresponds to the ratio of the empty-resonator frequency differences between fundamental and

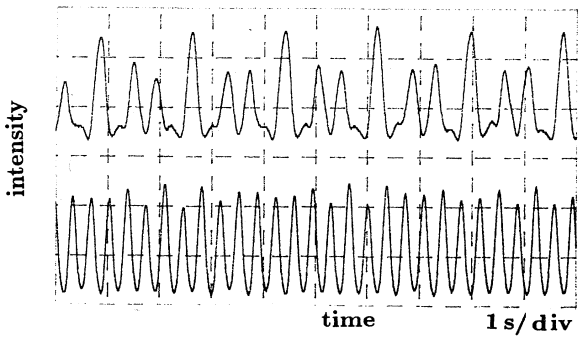

FIG. 18. Intensity at points on inner circle (upper trace) and outer circle (lower trace) of Fig. 17(a).

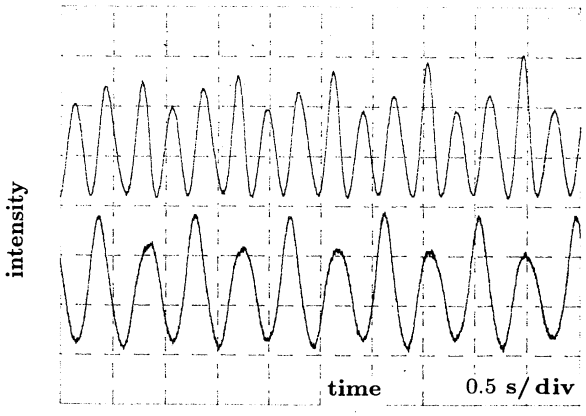

FIG. 20. Intensity on points of the two vortex trajectories of Fig. 19; upper trace: outer circle; lower trace: inner circle.

third-order transverse-mode family and, on the other hand, between fundamental and fifth-order mode family of the preceding FSR.

VI. CONCLUSION

We demonstrated various configurations of circling optical vortices in a photorefractive oscillator with BSO as the active material. At the low excitations used this system is equivalent to a class-A laser. The patterns can be qualitatively understood from simultaneous excitation of one or tow transverse modes together with a TEM_{00} mode or using a hydrodynamic analog for the laser. We observe hysteresis in the circling direction of the vortices, which may be related to the bistability of helical fields in lasers. It was possible to lock these modes of circular geometry, which do not lock in isotropic resonators. The transverse mode locking is in this case caused by resonator anisotropy. Locking of these modes corresponds to stopping the circular vortex motion.

ACKNOWLEDGMENTS

We would like to thank K. Staliunas, G. Slekys, and M. F. H. Tarroja for helpful discussions. M. Vaupel acknowledges financial support from the Friedrich Naumann Foundation.

[1] A. B. Coates *et al.*, Phys. Rev. A **49**, 1452 (1994).
[2] K. Staliunas, M. F. H. Tarroja, G. Slekys, C. O. Weiss, and L. Dambly, Phys. Rev. A (to be published).
[3] P. Yeh, *Introduction to Photorefractive Nonlinear Optics* (Wiley, New York, 1993).
[4] A. G. White *et al.*, J. Mod. Opt. **38**, 2531 (1991).
[5] K. Staliunas, Phys. Rev. A **48**, 1573 (1993).
[6] Chr. Tamm and C. O. Weiss, J. Opt. Soc. Am. **7**, 1034 (1990).

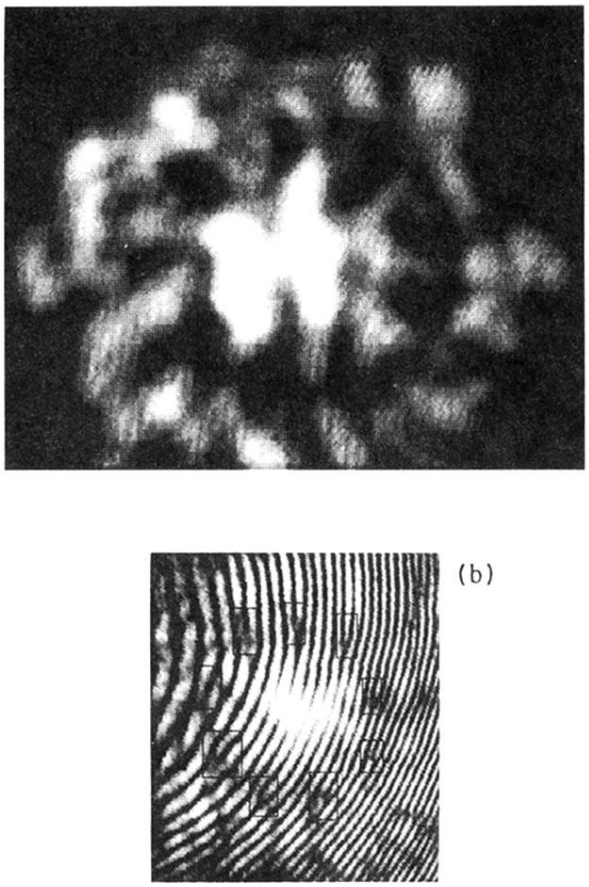

FIG. 10. Nine vortices circling (snapshot): (a) intensity and (b) interferogram.

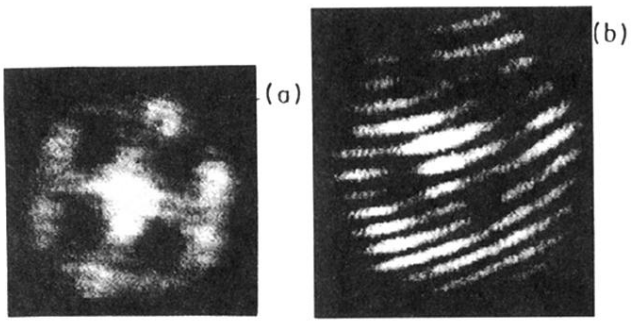

FIG. 12. Four circling vortices (snapshot): (a) intensity and (b) interferogram.

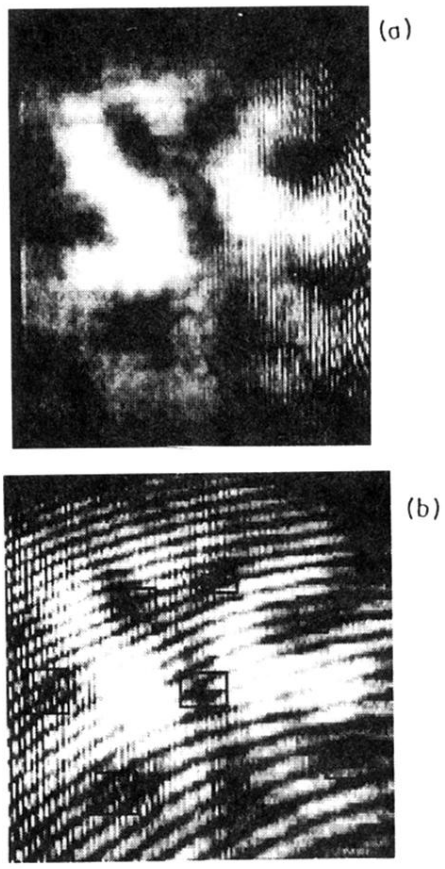

FIG. 16. Seven vortices circle around a central vortex (snapshot). The central vortex has topological charge opposite to the circling vortices. (a) intensity and (b) interferogram.

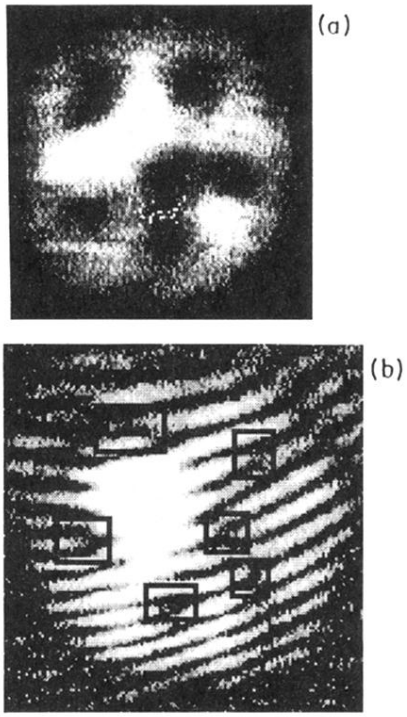

FIG. 17. Five vortices moving on an outer circle and one vortex moving in the same sense on a smaller circle concentric with the outer circle (snapshots). Topological charge of inner moving vortex opposite to outer vortices: (a) intensity and (b) interferogram.

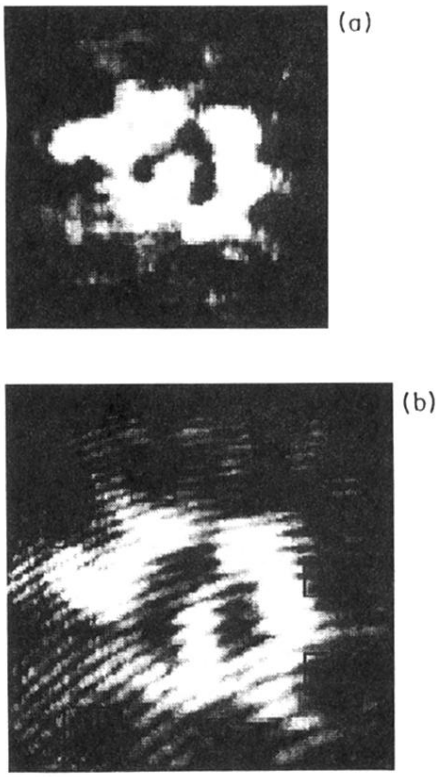

FIG. 19. Three vortices moving on an inner circle and eight vortices moving on an outer circle (snapshots): (a) intensity and (b) interferogram.

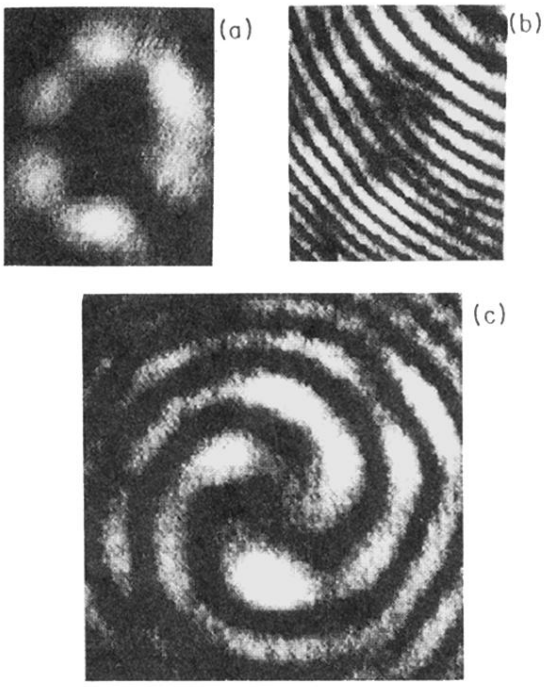

FIG. 3. Pattern with three phase singularities (vortices): (a) intensity, (b) interferogram with dislocations at the vortex locations, and (c) "spiral" interferogram of pattern with charge-3 phase singularity.

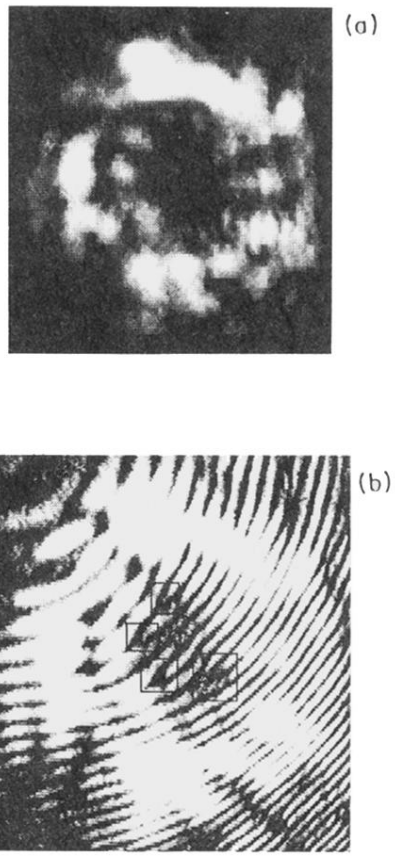

FIG. 4. Pattern with five phase singularities (vortices): (a) intensity and (b) interferogram with dislocations at the vortex locations.

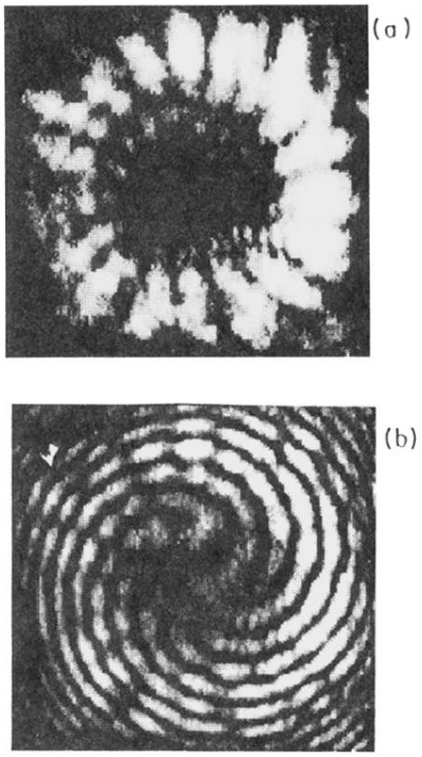

FIG. 5. Pattern with nine phase singularities (vortices): (a) intensity and (b) "spiral" interferogram of pattern with charge-9 phase singularity.

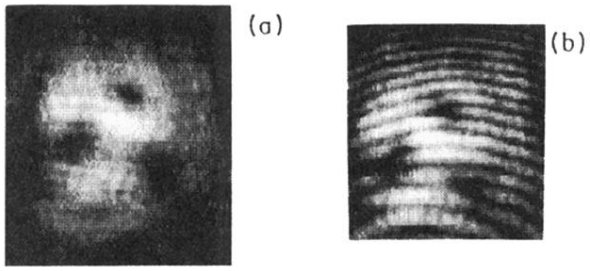

FIG. 6. Snapshot of three circling vortices: (a) intensity and (b) interferogram.

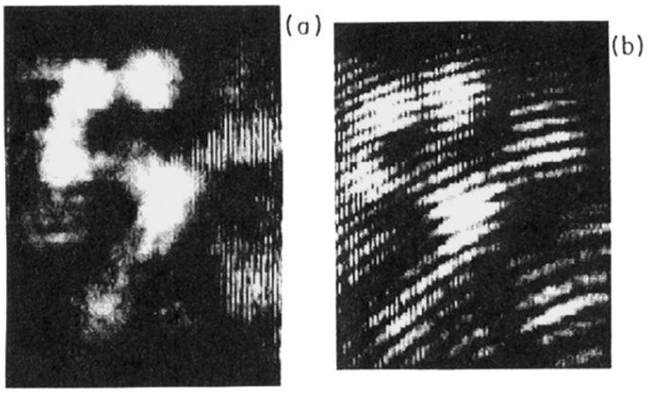

FIG. 8. Five circling vortices (snapshot): (a) intensity and (b) interferogram.